Lignin effect in castor oil-based elastomers: Reaching new limits in rheological and cushioning behaviors

Antonio M. Borrero-López [a,*], Ling Wang [b], Concepción. Valencia [a], José M. Franco [a], Orlando J. Rojas [b,c]

[a] *Pro²TecS – Chemical Process and Product Technology Research Centre. Dept. Ingeniería Química. ETSI. Universidad de Huelva. 21071 Huelva. Spain.*

[b] *Department of Bioproducts and Biosystems, School of Chemical Engineering, Aalto University, P.O. Box 16300, FIN-00076, Espoo, Finland.*

[c] *Bioproducts Institute, Departments of Chemical and Biological Engineering, Chemistry and Wood Science, 2360 East Mall, The University of British Columbia, Vancouver, BC V6T 1Z3, Canada.*

** Corresponding author (AB): e-mail: am.borrero@diq.uhu.es, phone: +34959217633*

ABSTRACT

Lignin is demonstrated as an unprecedented reinforcing material that tailors the rheological and cushioning properties of castor oil-based polyurethane elastomers, expanding their viscoelastic moduli by four orders of magnitude. The tensile strain at break was triplicated in the presence of lignin while the Young modulus and the stress at break were enhanced 17- and 7-fold, respectively. Remarkably, in compression tests, lignin addition increased the stresses at break by more than 88-fold, whereas the strain at failure shifted from 50 to 93%. Dynamic mechanical compression tests indicated outstanding cushioning and resistance performance. Overall, the results demonstrate a performance not reached before for biosourced elastomeric materials, fitting the demands of a wide range of applications.

Keywords: A. Polymer-matrix composites, A. Particle-reinforcement, B. Rheological properties, D. Mechanical testing, Bio-based composites.

1. INTRODUCTION

Owing to factors such as resource sufficiency and the need for greener materials, there is a high demand for biobased materials that are able to substitute or enhance those based on non-renewable sources [1]. According to the biorefinery concept, chemical intermediates and end-use materials can be produced in an integrated industrial process under the principles of green chemistry and engineering [2]. As a by-product of cellulosic pulp production, lignin may play a fundamental role since it is otherwise combusted for energy and chemical recovery [3]. Its production, amounting >50 million tons annually, makes lignin a widely available and low-cost bioresource suitable to substitute or partially replace non-renewables in given applications [4]. For instance, lignin possesses abundant functional groups, such as phenolic and aliphatic hydroxyl, carbonyl, carboxyl and methoxyl groups, which are available throughout a complex aromatic macromolecular structure [5], combining main phenylpropane units, namely, syringyl, guaiacyl and p-hydroxyphenyl. Technical lignin has been proposed as a key component or intermediate for end-use products, such as lubricating greases [6,7], foams [3], adhesives, coatings, or fine chemicals, among others [8].

Lignin has been used as a component in polyurethanes based on non-renewable polyols but full replacement of the latter, i.e., as the main component, has been challenging [3]. Moreover, environmentally friendly, fully biosourced and biodegradable or partially biodegradable bioproducts have considered composites of lignin with castor oil [6,7,9], poly (ε-caprolactone) [10] or polylactic acid [11], all of which replace petroleum-based counterparts while maintaining the expected

performance. Specially, compared to other vegetable oils, castor oil displays a high viscosity and thermal stability. Its low cost, availability and purity make castor oil a significant alternative precursor for bioproducts and biochemicals [12]. Combined with lignin, the hydroxyl groups present in castor oil's fatty acid chains make them attractive as polyol source in polyurethanes (PU). Depending on diisocyanate type, processing, and composition, lignin- and castor oil-based PUs allow a great range of possible materials and applications, including oleogels, thermoplastics, elastomers, films, foams or composites [6,7,13–16]. In particular, owing to their cushioning and resilience properties, related elastomers have been applied for flooring (sport indoor courts), footwear, surfboards, car interiors and household products [17]. Nonetheless, castor oil-based PU elastomers generally exhibit poor mechanical performance due to the dangling fatty acid chains of triglycerides [18]. The mechanical properties, however, can be adjusted considering the soft segments (SS) (basically castor oil domains) and hard segments (HS) (urea/urethane bonds) in PUs, with a superior strength observed at lower thermodynamic compatibility [18]. Upgrading the HS content may be possible by increasing diisocyanate concentration; unfortunately, this comes at the cost of reduced ductility [18,19]. As a consequence, nanoparticles, natural compounds, ceramic platelets and biopolymers have been used as fillers to adjust the crosslinking density needed and to increase both strength and resistance [19–21]. It is in this domain where lignin can play a determining role, e.g., acting as reinforcement in the PU structure and improving the mechanical properties [3,17]. Jeong et al. [16] developed polyethylene glycol (PEG) and acetylated lignin-based PUs with outstanding elastomeric properties, whose elongations at break were > 2000%. Likewise, Zhang et al. [22] proposed PEG-based PU elastomers with excellent tensile properties using oxidized lignin as copolymer. By

using polypropylene glycol as copolymer, Lang et al. [23] demonstrated lignin addition of up to 60% to increase the elastomeric viscoelastic functions, by up to six-fold, compared to the lignin-free system. In the search for fully-renewable copolymers, castor oil alone led to PUs with relatively poor elastomeric properties, with elongations < 130% [12–15]. However, improved tensile properties were found by combining castor oil with polycaprolactone [24] or PEG [25,26]. Moreover, castor oil- and lignin-based elastomers crosslinked with diphenylmethane-4,4′-diisocyanate (MDI) showed good tensile results, but mainly when castor oil was chemically modified to increase the hydroxyl index [13]. Despite these advances, no reports exist on the mechanical evaluation of related elastomers considering the response to static and dynamic compression, relevant to cushioning applications. Indeed, energy loss, compressibility and elongation, recoverability after strain and fatigue endurance are some of the main properties needed in suitable cushioning elastomers.

In this study, castor oil, lignin and hexamethylene diisocyanate (HDI) were used as oleo-based, eco-friendly and efficient PU elastomer. The rheological and cushioning properties were investigated, in light of the role of lignin compared to other well-known fillers (such as cellulose and silica nanoparticles).

2. MATERIALS & METHODS

2.1. Materials. Castor oil, hexamethylene diisocyanate (HDI), silica nanoparticles (40-63 μm), toluene and triethylamine were purchased from Merck (Finland) and used as received. Indulin AT, a purified form of kraft pine lignin, in the following referred only as lignin, was obtained from MeadWestvaco (USA). Detailed information about it can be found elsewhere [27]. Cellulose was directly obtained by milling paper produced from softwood (pine) fibers.

2.2. Lignin functionalization and preparation of the oleo-PU. The oleo-PUs were produced by following a two-step process [7], with lignin first functionalized with HDI, and subsequently dispersed in castor oil (see **Fig. 1**). In brief, in the first step, 100 mL toluene and a certain amount of lignin were introduced and sealed in a three-neck round bottom flask. Following, a 30-min conditioning that removed residual moisture was carried out by sparging nitrogen into the lignin-toluene system. HDI and triethylamine catalyst were then added. The concentrations of the HDI (8.33-25 wt%) and the catalyst (1/1 HDI/catalyst w/w ratio) were varied in order to investigate their effect on the mechanical properties of the ensuing PUs. The mixture was maintained for 24 hours at room temperature under vigorous agitation, followed by rotary evaporation to recover toluene and the catalyst (80ºC), resulting in the functionalized lignin. In a second step, the functionalized lignin was immediately introduced in a 100 mL stainless-steel reactor together with castor oil, and the mixture was gently stirred at 70 rpm by using a magnetic stirrer (RW 20 model, IKA, Germany) for another 24 hours at room temperature. Once the process was completed, the mixture was poured into molds for curing (one month) and to completely purge any remaining isocyanates in the mixture. The respective oleo-polyurethane sample ("oleo-PU" or, for simplicity, "PU") was then subjected to mechanical and rheological characterization. The preparation of the reference sample (lignin-free polyurethane), termed herein as "PU0", was carried following the same procedure described above, except for replacing lignin in this first step with an equivalent amount of castor oil (1/2 castor oil/HDI w/w ratio in this case).

Lignin loading (4.16-16.67 wt%) was adjusted with respect to castor oil, to evaluate its role and to compare the obtained PUs with the reference as well as those obtained by using other fillers, namely, silica nanoparticles and cellulose (8.33 wt%, 1/2 filler/HDI

ratio). The samples studied are listed in **Table 1**, and referred to as "PUX(Y)" where "X" represents the lignin concentration and "Y" the lignin/HDI w/w ratio.

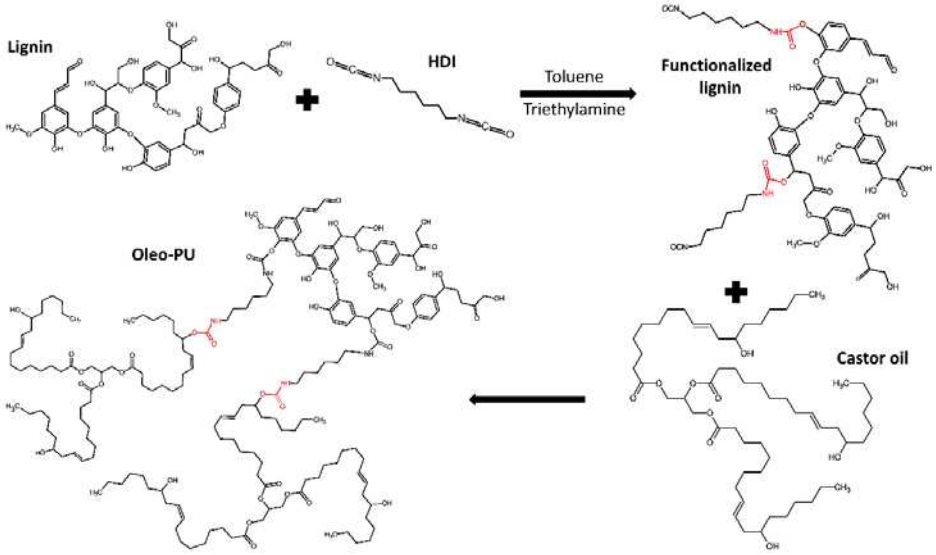

Fig. 1. Reaction scheme for lignin functionalization and oleo-PU formation through crosslinking with castor oil. The urethane links formed in each step are marked in red.

Table 1. Composition of the oleo-PUs.

Sample	Castor oil (wt%)	Lignin (wt%)	HDI (wt%)
PU0	83.33	0	16.67
PU8(1/2)	75.00	8.33	16.67
PU4(1/4)	79.16	4.16	16.67
PU17(1/1)	66.66	16.67	16.67
PU8(1/1)	83.34	8.33	8.33
PU8(1/3)	66.66	8.33	25.00
		Cellulose (wt%)	
CEL-PU	75.00	8.33	16.67
		Silica nanoparticles (wt%)	
SIL-PU	75.00	8.33	16.67

2.3. Characterization. The thermal stability of the different samples was assessed by thermogravimetry (Q500 thermal analyser, TA Instruments, USA). The testing protocol used heating to 600 ºC (10 ºC·min^{-1}), with a conditioning step at 30 ºC. The experiments were performed under nitrogen atmosphere.

Fourier transform infrared spectroscopy (FTIR) measurements were collected by using a Nicolet 380 FT-IR (Thermo Scientific, USA) spectrometer. Measurements were performed from 500 to 4000 cm^{-1} wavenumbers with a resolution of 4 cm^{-1}.

Differential scanning calorimetry (DSC) spectra were obtained by using a Q100 equipment (TA Instruments, USA). In order to eliminate the thermal history, a cycle was first applied by heating the sample from -80 to 250 ºC (10 ºC·min^{-1}) followed by cooling to -80 ºC at the same rate. Immediately thereafter, a new heating cycle was performed.

The surface topography of the PU samples was analyzed by means of field emission scanning electron microscopy (SEM) using a Zeiss Sigma VP microscope (Carl Zeiss Microscopy Ltd, UK). Prior to imaging, the samples were sputter-coated with 6 nm-thick gold layer.

The water contact angle (WCA) of the PUs was measured with a force tensiometer (Sigma 70, UK) equipped with a COHU solid-state CCD monochrome camera. A 6 μL water droplet was placed on the surface of the PUs, and the angle was carefully calculated by using the OneAttension software.

Strain sweeps, small-amplitude oscillatory shear and torsional (SAOS and SAOT) tests at different temperatures, and temperature sweeps were performed by using an Ares-G2 (TA Instruments, USA) equipped with either a rough plate-plate or a torsional geometry, depending on the consistency of the sample. The temperature was controlled by using a convection oven coupled to the rheometer. Generally, SAOS & SAOT tests were carried out between 0.03 and 100 rad·s^{-1}, at 25 ºC, and eventually at higher constant temperatures, in the range of 40-200 ºC. For the temperature sweeps (1 rad·s^{-1}), a constant heating ramp (1 ºC·min^{-1}) was applied from 30 ºC to 200 ºC, followed by a cooling step at the same decreasing rate, down to 30 ºC. The rheological tests were carried out within the linear viscoelastic range, previously identified by performing strain sweeps at the lowest and the highest temperatures.

Static tensile and compression tests were performed indistinctly in an AG-IS Universal Testing Machine (Shimadzu, Japan) and a 4204 Universal Tester (Instron, USA). Rates of 10 and 5 mm·min^{-1} were applied for the tensile and compression tests, respectively. Different load cells, from 1 kN to 10 kN, were used depending on the toughness of the sample. The compression results were well fitted to the model of Bian et al. (2018) [28]:

$$\sigma_c = A \cdot (e^{B \cdot \gamma_c} - 1) \quad (1)$$

where A and B are fitting parameters and γ_c represents the compressive strain of the sample.

Dynamic mechanical compression analyses were carried out using a TA.XT Plus Texture Analyser (Stable Micro Systems, UK). Given loads (0.35-0.70 MPa) and test lengths (70 s to 24 h) were applied at a constant compressive rate of 0.5 cycles·s^{-1}. The cushioning performance, determined as the energy the system is able to dissipate per unit area, was evaluated by the cushioning factor (CF) [1]:

$$CF = \frac{T \cdot L}{E} \quad (2)$$

where T is the initial thickness of the test specimen, L the load at the maximum strain applied and E the required energy to produce the deformation (area under the curve of the load applied vs. the strain achieved), respectively.

3. RESULTS and DISCUSSION

3.1. Thermogravimetric and FTIR analysis. The thermal decomposition profiles and FTIR spectra of castor oil and lignin, the functionalized castor oil and lignin, both at 1/2 biosource/HDI weight ratio, and the PU0 and PU8(1/2) systems are described in detail in the Supporting Information document. Compared to the functionalized castor oil, and due to the higher –OH group content, a lower free HDI content (and

consequently a higher crosslinked structure) was observed in the thermograms of the functionalized lignin (see **Fig. S1** and **Table S1,** Supporting Information). The results were related to the thermogravimetric observations of the corresponding oleogels with the free HDI content in the functionalized specimens tracking with the HDI available during the second step. Therefore, a more extensive crosslinking during the second step was achieved at a higher remaining free HDI content, which resulted in greater mass loss at temperatures higher than those corresponding to the main loss event, characteristic of the non-modified castor oil. The urethane formation was likewise confirmed in the FTIR spectra of functionalized castor oil and lignin, by observing the new peaks emerging from N–H stretching vibration (see **Fig. S2**). Moreover, the intensity of the peak at around 2270 cm^{-1} in the oleo-PU spectra allowed to follow the curing process and to ensure a complete reaction of free isocyanates.

3.2. Microstructural and topographical analysis. SEM micrographs of both the surface and the cross section of selected oleo-PUs are displayed in **Fig. S3**. Quite smooth surfaces were observed for both PU0 and PU8(1/2), with some small clusters apparent at low magnifications. Nonetheless, some large features also appeared for PU8(1/2), which became more prominent in cross section images, as a consequence of the colloidal size of the lignin [27]. Some cracks were identified, especially in PU8(1/2). However, images obtained at higher magnification showed more uniform and homogeneous microstructures for PU8(1/2), considering both surface and cross sections. These observations suggest a compatibilizing effect of lignin, in agreement with results for other types of lignin-containing PUs [29].

The WCA for the surface and cross sections are reported in **Table S1**. A higher WCA (9-10%) was recorded for the surface compared to the cross section, reflecting a

more hydrophilic composition in the core of the PU. Unexpectedly, PU0 showed a hydrophilic character (WCA<90 ºC), indicating that the addition of HDI to the castor oil matrix increased the surface energy of the mixture, as previously reported [30]. The hydrophobic character in the PU structure was partially recovered in the presence of lignin, probably due to the contribution of the aromatic skeleton and the random assembly of hydrocarbons, especially on the surface, where WCA > 90º [31], even though the core still remained hydrophilic.

3.3. Rheological behavior. The mechanical and rheological properties of the oleo-PU elastomers varied over a broad range, depending on the HDI, lignin and castor oil concentrations (**Table 1**). In particular, as shown in **Fig. 2,** the values of the storage, G' and the loss, G" moduli in the linear viscoelasticity regime spanned over a four-order of magnitude (note that pure elastomeric materials are included in **Fig. 2a**, whereas those showing a distinctive soft gel-like behavior are shown separately in **Fig. 2b)**. The visual appearance of the oleo-PUs is shown in **Fig. S4** (Supporting Information).

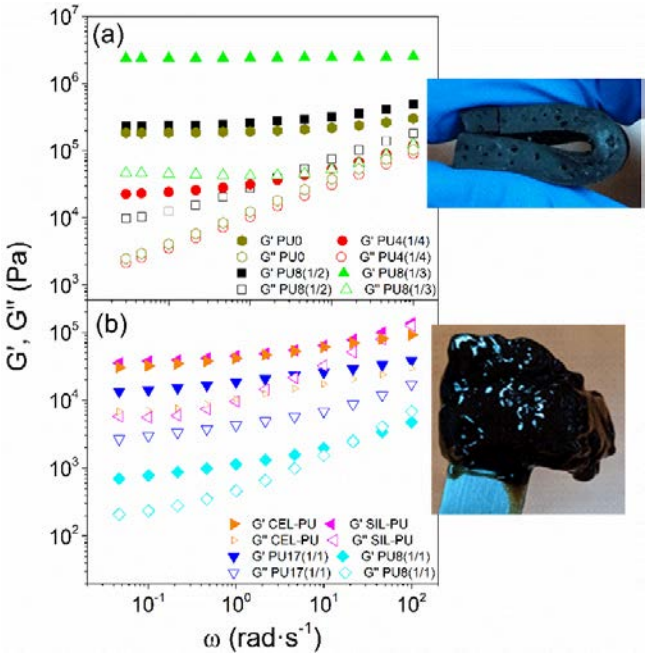

Fig. 2. Evolution of linear viscoelastic moduli with oscillatory frequency at 25 ºC for the castor oil-based oleo-PU (PU0), and those reinforced with either lignin, cellulose (CEL-PU) or silica nanoparticles (SIL-PU). Samples showing elastomeric behavior

(**Fig. 2a**) and soft or gel behavior (**Fig. 2b**) are shown. Selected photos for each system are also included to illustrate the differences (PU8(1/2), and PU8(1/1) respectively).

We compare the PU0 and PU8(1/2) samples to evaluate the effect of partial replacement of castor oil with lignin: slight differences in the storage moduli were noted, although the relative elastic response was slightly enhanced in PU0 (lower G"). The addition of lignin likely hindered castor oil structuration and hence crystallinity, thus providing lower relative elasticity to the system [32]. Nonetheless, it is worth mentioning that strain sweeps performed with PU8(1/2) in the torsional mode demonstrated outstanding flexibility of the specimen. **Video S1** (Supporting Information), for example, shows a sample withstanding up to 720º counter- and clockwise twisting without breaking. As shown in the thermogravimetric spectra (**Fig. S1**), a higher free-HDI content was present in PU0 for reaction during the second preparation step (**Fig. 1**), which likely increased crosslinking, favoring the ultimate elastic response.

Taking PU8(1/2) as a reference for the lignin-based systems, we note that an increase in the lignin content, to achieve lignin/HDI ratio of 1 (sample PU17(1/1)), failed to reach the desired elastomeric properties, as a consequence of the lower free –NCO content available for reaction with the castor oil during the second step. Indeed, similar behavior was observed for PU8(1/1), with a lower lignin content but the same lignin/HDI ratio. As a result, both PU17(1/1) and PU8(1/1) produced gel-like dispersions that are better suited for other applications, as previously reported [6,7]. In contrast, a higher relative diisocyanate content was obtained by decreasing the lignin content in the sample (PU4(1/4) with lignin/HDI ratio reduced to 1/4), which is expected to favor crosslinking. However, the viscoelastic properties did not reach the values as those found for 1/2 lignin/HDI ratio. This observation can be explained by

considering the possible high crosslinking degree achieved during the first preparation step, which reduced the compatibilization of the functionalized lignin with castor oil during the second step, as already shown in the case of other, more reactive diisocyanates [7].

When the HDI concentration was increased, for a given lignin content, a more fully developed plateau zone was observed for the viscoelastic moduli, with much higher values, implying an enhanced elastic response (the storage and loss moduli differed by almost two orders of magnitude, see PU8(1/3) in **Fig. 2a**). As expected, a higher HDI concentration improves crosslinking [18,19].

Cellulose and silica nanoparticles, which are well-known oil-structuring agents [33] were tested at a filler/HDI ratio of 1/2 (**Table 1**) and compared with the results obtained with lignin. Noting that the viscoelastic moduli of the oleo-PUs obtained with cellulose and silica (CEL-PU and SIL-PU, respectively) were comparable to those of PU4(1/4) (**Fig. 2b**), the performance is clearly lower, in terms of stiffness and elasticity, compared to the lignin counterparts (**Fig. S4**). The results highlight the comparatively better effect of lignin as a reinforcing agent.

The thermo-rheological response of the elastomers was determined to explore potential applications. As such, the PU8(1/2) sample was subjected to oscillatory torsional deformation (SAOT) in the 25-200 ºC range (**Fig. 3**). In general, a similar frequency dependence was found in the temperature range evaluated, especially below 140 ºC (**Fig. 3a** and **3b**). As can be observed, similar storage modulus values were achieved in the range of temperatures 25 to 40 ºC as well as 80 to 140 ºC. In contrast, a significant drop was observed from 40 to 80 ºC and above 140 ºC, which suggests an alteration of the elastomeric structure at those temperatures. The DSC spectrum (**Fig.**

S5, Supporting Information) confirms the presence of two glass transition temperatures centered around 55 and 171 ºC, related to HDI [34], which explains the dramatic drop in the viscoelastic functions. These results have been observed for large block polyurethanes due to microphase separation [35]. The evolution with frequency of both viscoelastic functions, up to 200 ºC, has been supplemented with a temperature sweep (1 rad·s^{-1}), as shown in **Fig. 3c**, which confirmed reduced G' values in the ranges 45-80 ºC and 160-185 ºC. The assessment of the temperature effect on the rheological properties of the elastomer was also considered by running a subsequent cooling ramp, from 200 ºC down to room temperature. As can be observed in **Fig. 3c**, the viscoelastic functions were drastically affected by the application of heating/cooling cycles, with no recovery of the initial values. Instead, G' at 200 ºC was maintained during cooling, whilst the G" followed a similar trend compared to the increasing temperature ramp, but yielding lower values. Therefore, the relative elastic properties of the sample were dramatically reduced upon restoring room temperature conditions, with a shift of the loss tangent (G"/G') from 0.11 to 0.23.

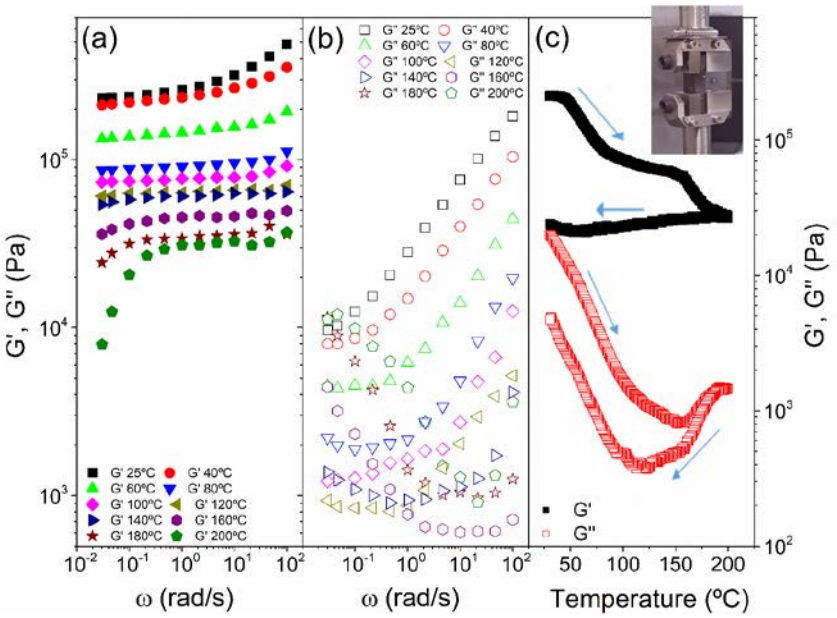

Fig. 3. Frequency-temperature dependence of the (a) storage and (b) loss moduli, within the 25-200 ºC range. (c) Evolution of G' (■) and G" (□) for the PU8(1/2) sample

undergoing subsequent heating (up to 200 ºC) and cooling (down to 25 ºC) cycles. The arrows indicate the time-evolution of the heating-cooling test. Inset: photograph of the sample in the torsional geometry during the test.

3.4. Mechanical performance. The mechanical properties of the oleo-PU elastomers were evaluated by performing static compression and tension tests. The compression profiles of the oleo-PU elastomers showed a variety of compression responses, depending on lignin, castor oil and HDI contents (see **Fig. S6)**. All the elastomers exhibited an exponential increase of the compressive stress [36], σ_c, which follows equation 1. For comparison **Table 2** lists the *A* and *B* parameters of Eq, 1 along with the σ_c values when reaching 20% and 50% strain and at failure.

Table 2. Mechanical performance of elastomers in compression tests (data include the average value and standard deviation).

Sample	Compression parameters, Eq. 1		Stress at 20% strain (MPa)	Stress at 50% strain (MPa)	Stress at failure (MPa)	Strain at failure (%)
	A (MPa)	B ($\%^{-1}$)				
PU0	0.150	0.036	0.16±0.01	0.75±0.07	0.76±0.09	50.7±0.90
PU8(1/2)	3.72E-4	0.132	0.13±0.02	0.72±0.07	67.3±9.86	93.7±1.14
PU4(1/4)	2.85E-3	0.089	0.01±0.01	0.13±0.08	3.08±0.15	88.6±0.44
PU8(1/3)	0.528	0.059	1.38±0.38	6.04±2.23	19.1±3.05	69.0±4.08

From the data in **Fig. S6** and **Table 2**, it is concluded that the lignin-free sample (PU0) exhibited the poorest mechanical performance, with < 50% strain and a very low compressive stress (0.76 MPa) causing total failure (**Video S2,** Supporting Information), despite the relatively high elasticity exhibited in oscillatory torsional tests performed inside the linear viscoelastic regime. When castor oil was partially replaced with lignin, a remarkable improvement in performance was observed. Related effects have been reported in the literature for lignin as a filler in elastomers [17]. The PU4(1/4) sample, with only a 4.17 wt% lignin, withstood > 88% strain without failure, associated to a compressive stress at break that is 4-times higher compared to the value observed for PU0 (3 MPa). Besides, the softer viscoelastic behavior determined in SAOT tests was

reflected in very low stress values needed to produce 20% and 50% strains. Doubling the lignin concentration (8.33 wt% lignin) endowed a substantially improved compressive mechanical response, as can be observed in PU8(1/2), where a compressive stress as high as ~67 MPa was necessary to break the sample, far better than that reported for other rubber or elastomeric materials [36,37] (see **Video S3**, Supporting Information) and comparable to high-impact composites based on alumina platelets [21]. Interestingly, the stress at 20 and 50% strain did not exceed those of PU0, demonstrating simultaneously a soft but very strong behavior at low and high deformations, respectively. We further note, however, that the mechanical properties were compromised at the highest lignin content, such as in the PU17(1/1) sample, which showed a gel-like rheological response, as previously discussed.

The influence of a higher crosslinking degree was analyzed by comparing PU8(1/2) and PU8(1/3) at differing HDI concentrations. As expected, a stiffer and more brittle material was produced by increasing crosslinking [18,19]. A higher compressive stress was needed from the very beginning to compress the sample, as observed by the higher values of stress at 20 and 50% strains, whereas failure took place at much lower values, 19 MPa stress and 69% strain.

According to the parameters in Eq. 1, the highest *B* values are associated with samples that are capable of holding higher strains without failure. On the other hand, *A* is associated with the slope of the initial trend compared to the final values, indicating PU8(1/2) with the lowest *A*, followed by PU4(1/4) and PU8(1/3), which is the strongest PU.

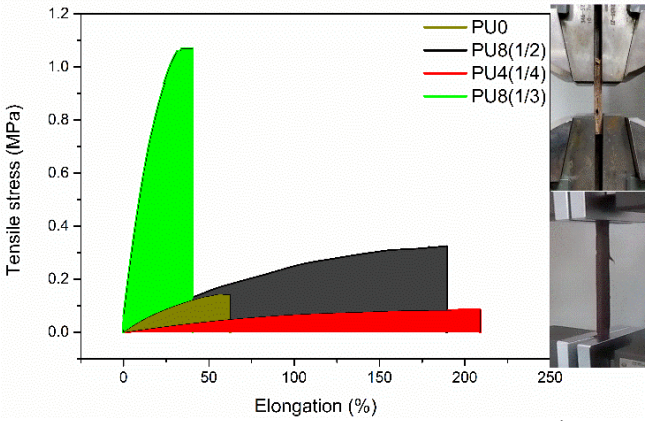

Fig. 4. Results of tensile tests (10 mm·min^{-1} elongation rate) comparing the average tensile profiles for the different elastomers. The different replicates have been included in **Fig. S7** (Supporting Information). Images of two elastomeric samples used in the tests (PU8(1/3), top and PU4(1/4), down) are included.

The oleo-PU elastomers were subjected to tensile tests (**Fig. 4** and **Fig. S7**). The tensile stress and elongation at break as well as Young modulus were determined (**Table 3)**. Apart from Zhang et al. (2019), who reported remarkable elongations (~120%) in tensile tests performed with castor oil-based PUs [15], the rather poor mechanical performance observed in our reference system (PU0) is in agreement with other studies, which have shown values of elongation at break lower than 32% [12–14]. As in the compression tests, partial substitution of castor oil with lignin resulted in a better performance; although, the elongational properties depended on lignin and HDI concentration, as already shown in the literature [13]. The PU4(1/4) sample (4.17 wt% of lignin) showed a significant improvement in elongation at break (209%), more than 3 times higher than that obtained in the absence of lignin (62%). However, the softer rheological characteristics demanded a lower stress for the completion of the failure, also exhibiting a lower value of the Young modulus. A strengthening of the systems occurred by increasing either the lignin or the HDI content (increasing both the Young modulus and the stress at break). This effect was more pronounced for the PU8(1/3) sample, as a consequence of the increased crosslinking, as previously discussed.

However, brittleness was severely compromised for the same reason, yielding much lower elongation at break [9,12]. Compared to PU4(1/4), the increased lignin loading in sample PU8(1/2) led to similar values of the strain at break, whereas higher Young modulus and stress at break were recorded. Even though the extensibility is still far from that found in other biocompatible composites especially designed for 3D printing [20], the results highlight the possibility of tuning the tensile properties according to the lignin content and lignin/HDI ratio, e.g., to fit the requirements of a given application.

Table 3. Average and standard deviation values of the Young modulus, tensile and elongation at break obtained from tensile tests.

PU elastomer	Young modulus (MPa)	Tensile stress at break (kPa)	Elongation at break (%)
PU0	0.42±0.02	145±11	63±8
PU8(1/2)	0.51±0.02	323±28	189±17
PU4(1/4)	0.10±0.02	80±9	209±42
PU8(1/3)	7.54±1.24	1118±172	35±14

3.5. Dynamic mechanical compression. Based on the compression and tensile results, PU8(1/2) was selected as the best elastomer for a wide variety of applications, and therefore we carried out a comprehensive study on the response of this system, to short- and long-term dynamic compression tests. **Fig. 5** summarizes the short-time responses to dynamic compression tests (0.70 MPa/200 kg equivalent force, 0.5 cycles/s, during 70 s) of PU8(1/2) and PU0. As can be observed, excellent recovery properties at short times were observed for PU8(1/2), from which only very slight variations in successive strain cycles were observed. In contrast, PU0 failed during the first cycle, showing a continuous strain increase up to the end of the test. A quite interesting feature was observed upon unloading of the elastomeric sample, namely, PU8(1/2) underwent reverse loops at high strains. This “catapult” phenomenon has been observed in nature and indicates a fast release of the absorbed energy [38].

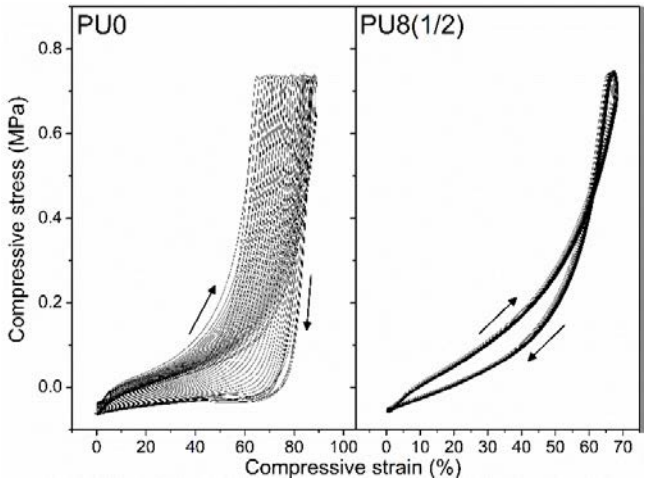

Fig. 5. Effect of lignin addition in the dynamic compression response of castor oil-based elastomer (PU0 and PU8(1/2)) evaluated in short-term (70 s) tests. Arrows are added to indicate successive compression cycles.

The effect of temperature and applied load in short-time dynamic compression tests can be evaluated from **Fig. S8** (Supporting Information). The higher the temperature or loading, the higher the maximum strains achieved, as can be expected considering the relatively strong influence of temperature on the rheological properties. Furthermore, the effect of temperature turned out to be more critical in samples subjected to lower loads.

We discuss next the influence of temperature and applied load on the long-term dynamic compression response of PU8(1/2). The evolution of the compressive strain was followed after the completion of the 24 h-tests at different temperatures and loads. A clear relationship between compressive strain and time (plotted in a logarithmic scale) is observed (**Fig. 6**).

The relationship between maximum compressive strains and time observed in **Fig. 6** is independent of the load applied, within the studied range, as very similar slopes were observed by applying 0.35 MPa and 0.70 MPa (100 or 200 kg force, respectively). Unlike load, the temperature noticeably affected the strain evolution with time, i.e., time effects became more limited at higher temperatures, possibly due to the softening of the

oleo-PU, as previously discussed. Some examples of cycles at different compression times are included in **Fig. S9**, which shows that the hysteresis loops did not change during the course of the tests [36]. This fact implies that the energy absorption of the material is not time-dependent, which substantially exceeds the results reported for other PU systems and commercial cushioning midsoles [16,39].

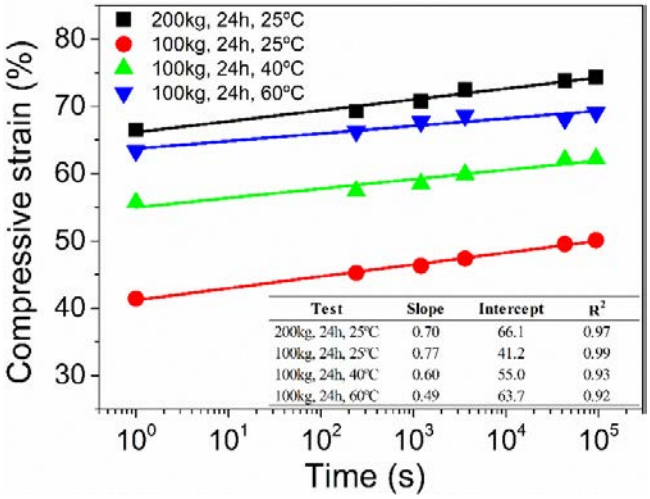

Fig. 6. Maximum compressive strains of PU8(1/2) with time during 24 h dynamic compression tests and measured under 100 (●) and 200 (■) kg compression loads at room temperature. Tests at 40 (▲) and 60 (▼) ºC under 100 kg are also included. Inset: Values of the slope, intercept and coefficient of determination of the fits.

Compression tests were also performed after the 24-hour essays in order to assess the fatigue effects in terms of mechanical properties. The compression remained unaltered for strains up to ca. 85%, after which failure started to occur (**Fig. S10**), slightly decreasing both the compressive stress and strain due to fatigue. However, these results are still far better than those reported for other cushioning materials [16,36].

The evolution of the energy loss during different short-time strain cycles was evaluated. As can be seen in **Fig. S11**, the PU8(1/2) system is able to release higher energy than provided at low strains, probably due to some structurally-stored energy. Both loading and unloading cycles became closer to each other when increasing the strain, as the mechanical spectra evolved following the typical hysteresis losses

exhibited by elastomers and rubbers, where a positive energy loss occurs [36]. Nevertheless, there is always a quick energy release immediately after unloading. We studied the evolution of the hysteresis losses, calculated by the difference between the areas under the compressive force curves in the loading and unloading cycles. Values from -12% up to 40% were recorded and plotted in **Fig. 6** for increasing strains, indicating that PU8(1/2) absorbed more energy under higher compression (**Fig. 6**). The energy absorption in our oleo-PU is similar to that reported for reference systems used as shoe soles for use under high loading [39].

In order to provide a quantitative reference to the cushioning properties, the cushioning factor (CF) was calculated from equation 2. Noting that CF < 8 is recommended for cushioning materials such as shoe soles [1], **Fig. 7** (inset table) indicates that PU8(1/2) fully met such performance, with deformations higher than 35%, indicating excellent cushioning under high loading.

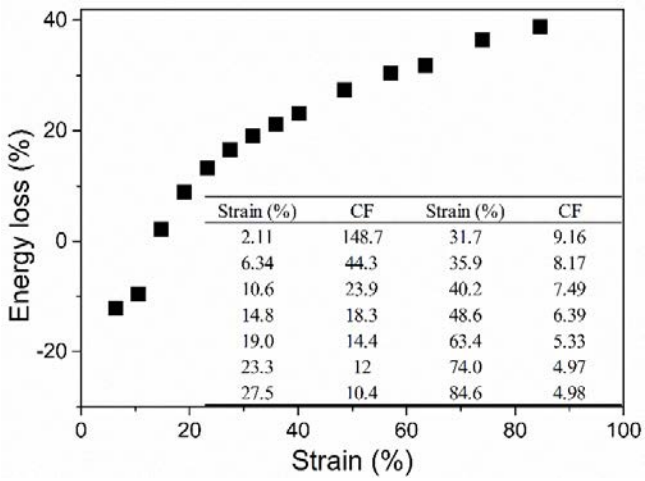

Strain (%)	CF	Strain (%)	CF
2.11	148.7	31.7	9.16
6.34	44.3	35.9	8.17
10.6	23.9	40.2	7.49
14.8	18.3	48.6	6.39
19.0	14.4	63.4	5.33
23.3	12	74.0	4.97
27.5	10.4	84.6	4.98

Fig. 7. Cushioning performance PU8(1/2): energy loss and cushioning factor (CF) (inset) as a function of the maximum strain applied.

4. CONCLUSIONS

We demonstrate the strengthening effect of lignin as a filler in castor oil/HDI elastomers. Despite the reduced elasticity observed from rheological measurements, the

addition of lignin promoted excellent performance as far as the tensile and compression behavior. Adjusting lignin or HDI concentration allows tailoring the rheological properties, from very soft to strong materials. The tensile strain at break of lignin-loaded polyurethanes was triplicated by replacing a small fraction of castor oil with lignin (4.17 wt%). At higher lignin content, 8.33 wt%, the PU maintained the elongation but presented 17- and 7-fold increases in the Young modulus and the stress at break, respectively. The increase in HDI concentration significantly enhanced the Young modulus and compressive stress at break with a simultaneous reduction of elongation. According to the compression tests, lignin addition (4.17 wt%) withstood > 88% strain without failure, an improvement of >38% compared to PU0, and exhibited a 4-times higher stress at break (3 MPa). A superior lignin addition (8.33 wt%), extended the outstanding properties, with a strain at failure of 93%, while the stress at break was 88-fold higher compared to the reference system, with values of 67 MPa, a record performance for biobased-polyurethane elastomers. Simultaneously, the sample exhibited similar stresses to produce 20 and 50% strains, thereby showing both soft and hard behavior depending on the strain applied. When isocyanate concentration was raised, higher stresses were needed to achieve 20 and 50% strains, however, the ultimate compressive strain was reduced. The optimum mechanical response was observed in elastomers with 8.33 wt% lignin and 1/2 lignin/HDI ratio. Such systems demonstrated outstanding short- and long-term dynamic compression properties, such as time-independent energy absorption evolution, outstanding resilience in long term high-load fatigue tests and a fast release of the absorbed energy during the compression. These facts make lignin-loaded oleo-PU formulations highly suitable as cushioning material for diverse applications.

ACKNOWLEDGMENTS

This work is part of a research project (RTI2018-096080-B-C21) sponsored by the MICINN-FEDER I+D+i Spanish Programme. A.M.B-L. acknowledges the Ph.D. Research Grant FPU16/03697 from MECD and EST17/00875 and EST18/00577 grants from MEFP which made possible the collaboration with the Aalto University.

REFERENCES

[1] M. Mukherjee, S.A. Gurusamy-Thangavelu, D.K. Chelike, A. Alagumalai, B.N. Das, S.N. Jaisankar, A.B. Mandal, 2020. Biodegradable polyurethane foam as shoe insole to reduce footwear waste: Optimization by morphological physicochemical and mechanical properties, Appl. Surf. Sci. 499, 143966. https://doi.org/10.1016/j.apsusc.2019.143966.

[2] S. Octave, D. Thomas, Biorefinery: Toward an industrial metabolism, Biochimie 91 (2009) 659–664. https://doi.org/10.1016/j.biochi.2009.03.015.

[3] S. Wang, W. Liu, D. Yang, X. Qiu, Highly Resilient Lignin-Containing Polyurethane Foam, Ind. Eng. Chem. Res. 58 (2019) 496–504. https://doi.org/10.1021/acs.iecr.8b05072.

[4] B.M. Upton, A.M. Kasko, Strategies for the conversion of lignin to high-value polymeric materials: Review and perspective, Chem. Rev. 116 (2016) 2275–2306. https://doi.org/10.1021/acs.chemrev.5b00345.

[5] M. Balakshin, E.A. Capanema, X. Zhu, I. Sulaeva, A. Potthast, T. Rosenau, O. Rojas, Spruce Milled Wood Lignin: Linear, Branched or Cross-linked?, Green Chem. 22 (2020) 3985–4001. https://doi.org/10.1039/D0GC00964D.

[6] A.M. Borrero-López, A. Blánquez, C. Valencia, M. Hernández, M.E. Arias, M.E. Eugenio, Ú. Fillat, J.M. Franco, Valorization of Soda Lignin from Wheat Straw Solid-State Fermentation: Production of Oleogels, ACS Sustain. Chem. Eng. 6 (2018) 5198–5205. https://doi.org/10.1021/acssuschemeng.7b04846.

[7] A.M. Borrero-López, C. Valencia, J.M. Franco, Rheology of lignin-based chemical oleogels prepared using diisocyanate crosslinkers: effect of the diisocyanate and curing kinetics, Eur. Polym. J. 89 (2017) 311–323. https://doi.org/10.1016/j.eurpolymj.2017.02.020.

[8] D. Kai, M.J. Tan, P.L. Chee, Y.K. Chua, Y.L. Yap, X.J. Loh, Towards lignin-based

functional materials in a sustainable world, Green Chem. 18 (2016) 1175–1200. https://doi.org/10.1039/c5gc02616d.

[9] M. Visanko, J.A. Sirviö, P. Piltonen, H. Liimatainen, M. Illikainen, Castor oil-based biopolyurethane reinforced with wood microfibers derived from mechanical pulp, Cellulose 24 (2017) 2531–2543. https://doi.org/10.1007/s10570-017-1286-x.

[10] R. Liang, J. Zhao, B. Li, P. Cai, X.J. Loh, C. Xu, P. Chen, D. Kai, L. Zheng, 2019. Implantable and degradable antioxidant poly(ε-caprolactone)-lignin nanofiber membrane for effective osteoarthritis treatment, Biomaterials 230, 119601. https://doi.org/10.1016/j.biomaterials.2019.119601.

[11] S.Y. Park, J.Y. Kim, H.J. Youn, J.W. Choi, Utilization of lignin fractions in UV resistant lignin-PLA biocomposites via lignin-lactide grafting, Int. J. Biol. Macromol. 138 (2019) 1029–1034. https://doi.org/10.1016/j.ijbiomac.2019.07.157.

[12] E. Hablot, D. Zheng, M. Bouquey, L. Avérous, Polyurethanes based on castor oil: Kinetics, chemical, mechanical and thermal properties, Macromol. Mater. Eng. 293 (2008) 922–929. https://doi.org/10.1002/mame.200800185.

[13] L.B. Tavares, C.V. Boas, G.R. Schleder, A.M. Nacas, D.S. Rosa, D.J. Santos, Bio-based polyurethane prepared from Kraft lignin and modified castor oil, Express Polym. Lett. 10 (2016) 927–940. https://doi.org/10.3144/expresspolymlett.2016.86.

[14] A. Cassales, L.A. Ramos, E. Frollini, Synthesis of bio-based polyurethanes from Kraft lignin and castor oil with simultaneous film formation, Int. J. Biol. Macromol. 145 (2020) 28–41. https://doi.org/10.1016/j.ijbiomac.2019.12.173.

[15] W. Zhang, Y. Zhang, H. Liang, D. Liang, H. Cao, C. Liu, Y. Qian, Q. Lu, C. Zhang, 2019. High bio-content castor oil based waterborne polyurethane/sodium lignosulfonate composites for environmental friendly UV absorption application, Ind. Crops Prod. 142, 111836. https://doi.org/10.1016/j.indcrop.2019.111836.

[16] H. Jeong, J. Park, S. Kim, J. Lee, N. Ahn, H. gyoo Roh, Preparation and characterization of thermoplastic polyurethanes using partially acetylated kraft lignin, Fibers Polym. 14 (2013) 1082–1093. https://doi.org/10.1007/s12221-013-1082-7.

[17] M. Alinejad, C. Henry, S. Nikafshar, A. Gondaliya, S. Bagheri, N. Chen, S.K. Singh, D.B. Hodge, M. Nejad, 2019. Lignin-Based Polyurethanes: Opportunities for Bio-Based Foams, Elastomers, Coatings and Adhesives, Polymers 11, 1202.

https://doi.org/10.3390/polym11071202.

[18] J. Zhang, M. Yao, J. Chen, Z. Jiang, Y. Ma, 2019. Synthesis and properties of polyurethane elastomers based on renewable castor oil polyols, J. Appl. Polym. Sci. 136, 47309. https://doi.org/10.1002/app.47309.

[19] X.P. An, J.H. Chen, Y.D. Li, J. Zhu, J.B. Zeng, Rational design of sustainable polyurethanes from castor oil: towards simultaneous reinforcement and toughening, Sci. China Mater. 61 (2018) 993–1000. https://doi.org/10.1007/s40843-017-9192-8.

[20] J.M. Koo, J. Kang, S.H. Shin, J. Jegal, H.G. Cha, S. Choy, M. Hakkarainen, J. Park, D.X. Oh, S.Y. Hwang, 2020. Biobased thermoplastic elastomer with seamless 3D-Printability and superior mechanical properties empowered by in-situ polymerization in the presence of nanocellulose, Compos. Sci. Technol. 185, 107885. https://doi.org/10.1016/j.compscitech.2019.107885.

[21] R.G. Crookes, H. Wu, S.J. Martin, C. Kay, G.W. Critchlow, 2019. Bio-inspired platelet reinforced elastomeric-ceramic composites for impact and high strain rate applications, Compos. Sci. Technol. 184, 107857. https://doi.org/10.1016/j.compscitech.2019.107857.

[22] Y. Zhang, R. Yan, T. dung Ngo, Q. Zhao, J. Duan, X. Du, Y. Wang, B. Liu, Z. Sun, W. Hu, H. Xie, Ozone oxidized lignin-based polyurethane with improved properties, Eur. Polym. J. 117 (2019) 114–122. https://doi.org/10.1016/j.eurpolymj.2019.05.006.

[23] J.M. Lang, U.M. Shrestha, M. Dadmun, 2018. The Effect of Plant Source on the Properties of Lignin-Based Polyurethanes, Front. Energy Res. 6, 4. https://doi.org/10.3389/fenrg.2018.00004.

[24] S.M. Hong, J.R. Cha, J.G. Kim, 2020. Preparation of body-temperature-triggered shape-memory polyurethane with biocompatibility using isosorbide and castor oil, Polym. Test. 91, 106852. https://doi.org/10.1016/j.polymertesting.2020.106852.

[25] Z. Gao, J. Peng, T. Zhong, J. Sun, X. Wang, C. Yue, Biocompatible elastomer of waterborne polyurethane based on castor oil and polyethylene glycol with cellulose nanocrystals, Carbohydr. Polym. 87 (2012) 2068–2075. https://doi.org/10.1016/j.carbpol.2011.10.027.

[26] S. Oprea, Dependence of fungal biodegradation of PEG/castor oil-based polyurethane elastomers on the hard-segment structure, Polym. Degrad. Stab. 95

(2010) 2396–2404. https://doi.org/10.1016/j.polymdegradstab.2010.08.013.

[27] M.A. Rahman, D. De Santis, G. Spagnoli, G. Ramorino, M. Penco, V.T. Phuong, A. Lazzeri, Biocomposites based on lignin and plasticized poly(L-lactic acid), J. Appl. Polym. Sci. 129 (2013) 202–214. https://doi.org/10.1002/app.38705.

[28] H. Bian, L. Wei, C. Lin, Q. Ma, H. Dai, J.Y. Zhu, Lignin-Containing Cellulose Nanofibril-Reinforced Polyvinyl Alcohol Hydrogels, ACS Sustain. Chem. Eng. 6 (2018) 4821–4828. https://doi.org/10.1021/acssuschemeng.7b04172.

[29] C.W. Park, W.J. Youe, S.Y. Han, J.S. Park, E.A. Lee, J.Y. Park, G.J. Kwon, S.J. Kim, S.H. Lee, 2019. Influence of lignin and polymeric diphenylmethane diisocyante addition on the properties of poly(butylene succinate)/wood flour composite, Polymers 11, 1161. https://doi.org/10.3390/polym11071161.

[30] A.D. Macalino, V.A. Salen, L.Q. Reyes, 2017. Castor Oil Based Polyurethanes: Synthesis and Characterization, IOP Conf. Ser. Mater. Sci. Eng. 229, 012016. https://doi.org/10.1088/1757-899X/229/1/012016.

[31] W. Horwath, Carbon Cycling: The Dynamics and Formation of Organic Matter, in: Paul, E. A. (Ed.), Soil Microbiology, Ecology and Biochemistry, fourth ed., Elsevier Inc., Amsterdam, 2015, pp. 339–382 https://doi.org/10.1016/b978-0-12-415955-6.00012-8.

[32] P. Mousavioun, P.J. Halley, W.O.S. Doherty, Thermophysical properties and rheology of PHB/lignin blends, Ind. Crops Prod. 50 (2013) 270–275. https://doi.org/10.1016/j.indcrop.2013.07.026.

[33] A.R. Patel, Alternative Routes to Oil Structuring, Springer, Berlin, 2015. https://doi.org/10.1007/978-3-319-19138-6.

[34] Q. Luo, J. Chen, P. Gnanasekar, X. Ma, D. Qin, H. Na, J. Zhu, N. Yan, A facile preparation strategy of polycaprolactone (PCL)-based biodegradable polyurethane elastomer with a highly efficient shape memory effect, New J. Chem. 44 (2020) 658–662. https://doi.org/10.1039/c9nj05189a.

[35] S. Velankar, S.L. Cooper, Microphase Separation and Rheological Properties of Polyurethane Melts. 1. Effect of Block Length, Macromolecules 31 (1998) 9181–9192. https://doi.org/10.1021/ma9811472.

[36] C. Delgado-Sánchez, G. Amaral-Labat, L.I. Grishechko, A. Sánchez-Sánchez, V. Fierro, A. Pizzi, A. Celzard, Fire-resistant tannin-ethylene glycol gels working as

rubber springs with tuneable elastic properties, J. Mater. Chem. A. 5 (2017) 14720–14732. https://doi.org/10.1039/c7ta03768f.

[37] K. Haraguchi, Synthesis and properties of soft nanocomposite materials with novel organic/inorganic network structures, Polym. J. 43 (2011) 223–241. https://doi.org/10.1038/pj.2010.141.

[38] R.M. Alexander, H.C. Bennet-Clark, Storage of elastic strain energy in muscle and other tissues, Nature 265 (1977) 114–117. https://doi.org/10.1038/265114a0.

[39] L. Wang, Y. Hong, J.X. Li, Durability of running shoes with ethylene vinyl acetate or polyurethane midsoles, J. Sports Sci. 30 (2012) 1787–1792. https://doi.org/10.1080/02640414.2012.723819.

FIGURE CAPTIONS

Fig. 2. Reaction scheme for lignin functionalization and oleo-PU formation through crosslinking with castor oil. The urethane links formed in each step are marked in red.

Fig. 2. Evolution of linear viscoelastic moduli with oscillatory frequency at 25 ºC for the castor oil-based oleo-PU (PU0), and those reinforced with either lignin, cellulose (CEL-PU) or silica nanoparticles (SIL-PU). Samples showing elastomeric behavior (**Fig. 2a**) and soft or gel behavior (**Fig. 2b**) are shown. Selected photos for each system are also included to illustrate the differences (PU8(1/2), and PU8(1/1) respectively).

Fig. 3. Frequency-temperature dependence of the (a) storage and (b) loss moduli, within the 25-200 ºC range. (c) Evolution of G' (■) and G" (□) for the PU8(1/2) sample undergoing subsequent heating (up to 200 ºC) and cooling (down to 25 ºC) cycles. The arrows indicate the time-evolution of the heating-cooling test. Inset: photograph of the sample in the torsional geometry during the test.

Fig. 4. Results of tensile tests (10 $mm \cdot min^{-1}$ elongation rate) comparing the average tensile profiles for the different elastomers. The different replicates have been included in **Fig. S7** (Supporting Information). Images of two elastomeric samples used in the tests (PU8(1/3), top and PU4(1/4), down) are included.

Fig. 5. Effect of lignin addition in the dynamic compression response of castor oil-based elastomer (PU0 and PU8(1/2)) evaluated in short-term (70 s) tests. Arrows are added to indicate successive compression cycles.

Fig. 6. Maximum compressive strains of PU8(1/2) with time during 24 h dynamic compression tests and measured under 100 (●) and 200 (■) kg compression loads at room temperature. Tests at 40 (▲) and 60 (▼) ºC under 100 kg are also included. Inset: Values of the slope, intercept and coefficient of determination of the fits.

Fig. 7. Cushioning performance PU8(1/2): energy loss and cushioning factor (CF) (inset) as a function of the maximum strain applied.

TABLES

Table 1. Composition of the oleo-PUs.

Sample	Castor oil (wt%)	Lignin (wt%)	HDI (wt%)
PU0	83.33	0	16.67
PU8(1/2)	75.00	8.33	16.67
PU4(1/4)	79.16	4.16	16.67
PU17(1/1)	66.66	16.67	16.67
PU8(1/1)	83.34	8.33	8.33
PU8(1/3)	66.66	8.33	25.00
		Cellulose (wt%)	
CEL-PU	75.00	8.33	16.67
		Silica nanoparticles (wt%)	
SIL-PU	75.00	8.33	16.67

Table 2. Mechanical performance of elastomers in compression tests (data include the average value and standard deviation).

Sample	Compression parameters, Eq. 1		Stress at 20% strain (MPa)	Stress at 50% strain (MPa)	Stress at failure (MPa)	Strain at failure (%)
	A (MPa)	B ($\%^{-1}$)				
PU0	0.150	0.036	0.16±0.01	0.75±0.07	0.76±0.09	50.7±0.90
PU8(1/2)	3.72E-4	0.132	0.13±0.02	0.72±0.07	67.3±9.86	93.7±1.14
PU4(1/4)	2.85E-3	0.089	0.01±0.01	0.13±0.08	3.08±0.15	88.6±0.44
PU8(1/3)	0.528	0.059	1.38±0.38	6.04±2.23	19.1±3.05	69.0±4.08

Table 3. Average and standard deviation values of the Young modulus, tensile and elongation at break obtained from tensile tests.

PU elastomer	Young modulus (MPa)	Tensile stress at break (kPa)	Elongation at break (%)
PU0	0.42±0.02	145±11	63±8
PU8(1/2)	0.51±0.02	323±28	189±17
PU4(1/4)	0.10±0.02	80±9	209±42
PU8(1/3)	7.54±1.24	1118±172	35±14